[SSC24-WIII-02]

# Big Red Sat-1: Mission Overview and Future Opportunities for Perovskites in Low Earth Orbit

Walker S. Arce, Vince Orsi, Nick Wayman, Joel Murch-Shafer, Karen Stelling
University of Nebraska-Lincoln
1700 Vine Street, Lincoln, NE 68588; (402) 472-3181
wsarcera@gmail.com

Robert Schmidt
Acellus Academy of Homeschooling
Lincoln, NE

Kelly Schutt, Joseph M. Luther
National Renewable Energy Laboratory
15013 Denver West Pkwy, Golden, CO 80401; (303) 384-6494

Hadi Afshari
Oklahoma University
660 Parrington Oval, Norman, OK 73019; (405) 325 0311

Ian Sellers
University at Buffalo
230 L Davis Hall, Buffalo, NY 14260; (716) 645-1152

## ABSTRACT

Perovskite solar cells are an emerging technology that holds the promise of reducing the size and weight of solar panels on satellites. While many research laboratories have produced perovskite solar cells and characterized their performance in laboratory conditions, few have endeavored to launch them into space. The Big Red Sat-1 (BRS-1) is one such satellite, designed to incorporate three different perovskite solar cell architectures along with custom curve tracing instrumentation for launch into low earth orbit through NASA's CubeSat Launch Initiative. The curve tracer is realized using a precision resistor ladder with high quality current and voltage measurements. Perovskite solar cell samples were fabricated by the National Renewable Energy Laboratory and characterized in their facilities before shipment. These cells were recharacterized using flight hardware before integration into the Nanoracks launcher. In addition to the eighteen perovskite solar cell pixels, a gallium arsenide (GaAs) solar cell was included to trigger measurements when the BRS-1 is pointing at the sun. During nominal operations, the BRS-1 will continuously take J-V curves while the GaAs solar cell is illuminated and will be in a low power state otherwise. Future missions should include a sun vector sensor for precise solar flux measurements, active curve tracing for dark current measurements, and explore alternative perovskite solar cell architectures including tandem cells. All designs for BRS-1 have been made open source to benefit other student-led missions. BRS-1 is currently in-orbit and transmitting measurement data.

## INTRODUCTION

From the silicon-solar cells used on Vanguard 1 in 1958 to the Gallium Arsenide (GaAs) solar cells used in Starlink satellites in 2024, inner Solar System satellites are linked to photovoltaic devices for long-term power generation.[1] Just as GaAs solar cells effectively replaced their silicon counterparts, researchers are searching for a replacement for GaAs. One candidate to replace GaAs is the perovskite solar cell, which was first reported on by Kojima et al. 2009, demonstrating an efficiency of 3.8%.[2] For the past fifteen years, researchers have improved the performance of perovskite solar cells, achieving effi-

ciencies of up to 26.1%.[3]

As NASA prepares humanity's return to the Moon as part of the Artemis program, larger solar power arrays need to be manufactured with resources that are either found on the lunar surface or carried by rocket.[4] In either case, the equipment for manufacture will also need to be transported to the lunar surface, so simpler manufacturing procedures and reduced material requirements are desired. Due to the simple manufacturing requirements of perovskite solar cells, on top of their self-healing, thermal cycling endurance, VUV endurance, and their defect tolerance, this technology has the potential to meet the needs of the Artemis mission.

To validate this technology in space conditions, we have devised an experiment integrated into a 1U CubeSat. Using custom instrumentation and current generation perovskite solar cells, our CubeSat, named Big Red Sat-1, will characterize these solar cells while in low earth orbit. By incorporating perovskite solar cells manufactured with different considerations and monitoring their changes in performance from manufacturing to operation in orbit, we can point towards a particular manufacturing procedure that is best suited for space operation.

Big Red Sat-1 was selected for launch by the NASA CubeSat Launch Initiate in April 2021, integrated into the NanoRacks CubeSat Deployer 27 in December 2023, launched to the International Space Station in March 2024, and is currently in orbit after being deployed in April 2024. This paper covers the current state of the art for perovskite solar cells, how Big Red Sat-1 was designed to assess their performance in a space environment, and what future missions should look to incorporate to continue towards the goal of low-cost, lightweight, solar power generation for future spacecraft.

## BRIEF PROJECT HISTORY

Big Red Sat-1 was initiated in August 2020 based on an idea presented to the Dean of the College of Engineering (CoE) at the University of Nebraska-Lincoln (UNL) for a team of Nebraska middle and high school students to develop a CubeSat under the mentorship of a faculty advisor and undergraduate engineering students. This project had a fast start with help from the Aerospace Club's Advisor, the Aerospace eXperimental Payloads (AXP) leads, and the CoE's Engineering Education and Outreach Coordinator, who put out a statewide call to science teachers across the state for middle and high school students with an interest participating in the program.

Students who responded were interviewed and team meetings started in September, despite COVID. Students were introduced to CubeSat and engineering concepts, while exploring potential research concepts. Students presented concepts to mentors and a Preliminary Design Review (PDR) was held in October. A proposal was submitted to NASA in December, and the team's proposal was selected in April of 2021. As funds were raised, students developed and advanced concepts, designs, sources, construction, programming and testing over the following years, while receiving support and reporting progress to NASA and Nanoracks (now Voyager Space).

There were core team members who participated throughout the project, new members with key skills, and changes in leadership and participants as the project progressed, however, the focus remained on creating a functional satellite to advance knowledge of perovskite solar cell performance in space. Big Red Sat-1 passed the vibration test and received the Certificate of Payload Functionality in November of 2023 and was integrated into the deployer in December of 2023 for manifest and launch to the ISS in March of 2024 on CRS-2 SpX-30, and was deployed from the ISS and operational on April 18, 2024.

## PEROVSKITE BACKGROUND

The term perovskite is used to identify a group of compounds with identical crystal structure to calcium titanium oxide ($CaTiO_3$).[5] To be considered a perovskite, it should be a compound with an ABX3 structure, where two cations of different sizes, "A" and "B", and one anion, "X", where "A" forms a cubo-octahedral structure with 12 "X" anions and "B" is confined by an octahedral site by 6 "X" anions, though there are numerous varieties with different properties.[6] Most modern perovskite solar cells are described by formamidinium lead iodide ($FAPbI_3$)-rich compositions, which were first reported by Jeon et al. 2018 with an efficiency of 18%.[7] This composition of perovskite solar cell has been found to exhibit a superior radiation tolerance in comparison to silicon and GaAs solar cells, surviving against 1 MeV of electrons and 50 KeV of protons.[8]

Various improvements can be made to this formulation by incorporating performance enhancing additives. For instance, thermal stress can be eliminated in the perovskite solar cell by incorporating an alkyl-ammonium additive.[9] Even changes to the packaging approach can aid the longevity of the per-

ovskite solar cell. Space conditions introduce unique environmental conditions such as atomic oxygen, where oxygen molecules are energized by UV radiation, can cause corrosion and the damage of metallic contacts. These molecules damage perovskite solar cells within 2 hours of exposure, causing a 43% reduction in power conversion efficiency[10] or the complete failure of the solar cell.[11] This effect could be mitigated by applying a thin silicon oxide (SiO) encapsulation, reducing the loss of efficiency by up to 80%, in comparison to samples without.[11]

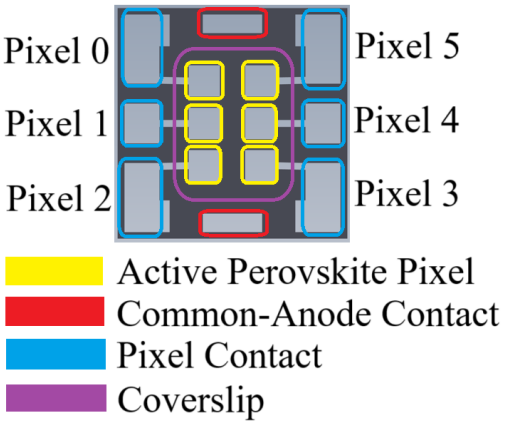


**Figure 1: Photomask of perovskite solar cells used in BRS-1 showing the active areas, contacts, and coverslip**

Perovskite solar cells can reasonably be designed for any layout compatible with their manufacturing process. Figure 1 shows the layout for the perovskite solar cells used in the BRS-1 satellite. The substrate has six pixels fabricated on it with larger metallic ohmic contacts for connection into an electrical system.

To characterize the performance of a solar cell a variable load is applied to the sample. While the sample is under illumination of a spectrum resembling AM1.5, a variable load sweeps the sample while collecting current and voltage measurements.[12] The load will sweep from open circuit condition (maximum voltage production) to short circuit condition (maximum current conduction), which when arranged on an X-Y plot of voltage vs. current density, generates a rounded knee plot in the first quadrant. To prevent undue load on the sample, voltage measurements should be conducted with a high input resistance. The current measurements are also commonly divided by the aperture area to calculate current density (J).

The current density-voltage (J-V) measurement system is crucial for determining overall health and performance of the solar cells. Any degradation to the solar cells will reflect a signature in the J-V results in the form of induced internal resistance against carrier extraction, damage to the band gap of the absorber material, or a loss of current density. The power conversion efficiency (PCE) of the solar cells is also extracted from the J-V results. In space, this system needs to be robust against the vacuum and temperature variations.

## SCIENCE MISSION OVERVIEW

BRS-1 is a 1U CubeSat designed to characterize the performance of three perovskite solar cells that are exposed to the low earth orbit environment. As perovskite solar cells increase in stability and reliability due to adjustments in construction, their ability to survive in space environments must be evaluated. Without this crucial step, two issues can arise. First, their technology readiness level (TRL) will not surpass TRL 6 (technology demonstration in relevant environment), limiting their ability to be used in emerging missions as a critical component, rather than as a technology demonstration. Second, perovskite development may fine-tune towards performance for terrestrial conditions and subsequently fail in space conditions, which has unique failure mechanisms. BRS-1 intends to move current generation perovskite solar cells from TRL 6 to TRL 7 by validating that these same cells are capable of handling low earth orbit conditions.

In addition to the proper BRS-1 mission, a physical twin of the perovskite payload was manufactured with perovskite solar cell samples produced from the same batch as the ones integrated into BRS-1. This physical twin will undergo simulated low earth orbit testing at UNL, where it will be exposed to similar levels of atomic oxygen and vacuum ultraviolet while maintained in a vacuum. Given the case where the samples in low earth orbit demonstrate a reduction in performance, the physical twin samples can be inspected for potential failure mechanisms.

The solar cells that are being monitored are three perovskite solar cells and a GaAs module. For the GaAs module, a small 'subpanel' of a standard 1U GaAs solar panel is constructed, so that only one third remains. This provides a useful reference to ensure that the system is operating as expected as well as a convenient way to trigger measurements. The GaAs module is connected to a comparator circuit that pulls a signal line low when its open circuit voltage rises above a given level. This occurs when the GaAs' polar angle, $\theta$, is $\pm 25^{\circ}$, so when this signal is active, the microcontroller is enabled to start

characterizing the system. The system will continue to sample until the GaAs is no longer facing towards the sun.

Perovskite solar cells are constantly modified regarding their structure and chemical formula to improve not only the PV performance but also to enhance the stability and application related properties. Perovskite solar cells benefit from a lack of $O_2$ and $H_2O$ in space applications, which rapidly degrade their performance when encapsulation is compromised. Studying the performance and degradation of perovskite solar cells at space have been performed in three main approaches:

(a) Solar cells mounted on balloons and sent to very high altitudes (a drawback of this approach is the limitation in altitude). The cells can be measured at high altitudes for their PV performance.[13,14] This is active testing of the performance of the cells.

(b) Mounted on the wings of the International Space Station (ISS), the cells were brought back to Earth after a few months to investigate the effect of space conditions on the PV performance of the solar cells. This is passive characterization. In this approach it is hard to figure out at which stage the solar cells start to degrade; it can be due to the launch conditions, pre-launch storage. This is passive testing of the performance of the cells.[15]

(c) Mounted on the CubeSats and measured their performance in-situ conditions. This is active testing, which is not limited by height, and the testing conditions are the same as practical conditions. It is far more accurate, and hence crucial, for the further development of space-grade solar cells than passive testing.[16,17]

The perovskite samples were manufactured by the National Renewable Energy Laboratory (NREL) and SwiftSolar. Each sample was encapsulated using a 100-micron SiO coverslip, which was adhered with a drop of EP30-2 epoxy. Before being shipped to the University of Nebraska-Lincoln (UNL), NREL characterized the performance of the samples using their Keithley equipment. The samples would be recharacterized by the UNL team using custom equipment, designed similarly to the equipment on BRS-1. The samples would be recharacterized after the Sine Sweep and Random Vibration Testing to assess if any damage or issues were caused by the simulated launch conditions. Providing the samples were still actively generating power, BRS-1 would be launched and deployed into orbit, where the performance of the solar cells would be compared to the on-ground performance over a period of 90 days.

## INSTRUMENT OVERVIEW

Measuring the performance of perovskite solar cells in space requires specialized instrumentation to assess their efficiency, stability, and degradation under extraterrestrial conditions. The instrumentation must be able to operate reliably in the harsh environment of space, where factors such as vacuum, radiation, extreme temperatures, and microgravity come into play. Although in passive testing the measurements are all performed at earth, and instrumentation does not need to be launched to space, but in order to acquire more accurate information on the effect of space conditions on the PV performance, the in-situ testing is a must which is far more informative.

Onboard BRS-1 is a machined aluminum perovskite retaining payload that has the capability to maintain a pressurized gas volume. This payload can retain three perovskite solar cell samples as well as an FSS100 Nano Fine Sun Sensor from Tensor Tech, serving as the sun vector sensor. Additionally, this payload is designed to mount a GaAs solar cell module that provides a known reference for our measurements.

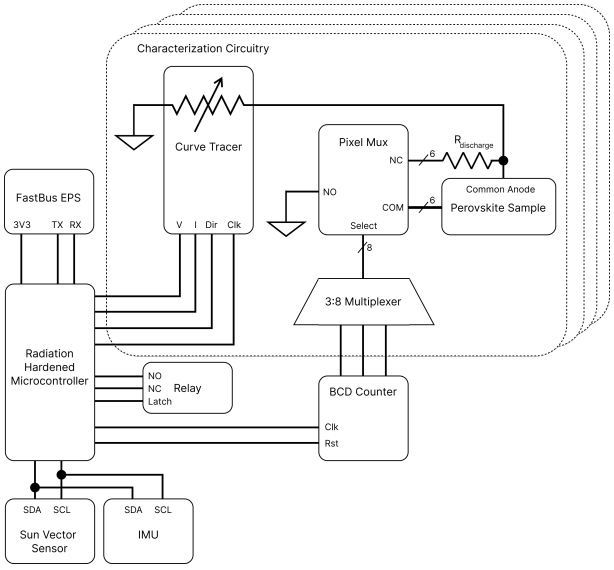


**Figure 2: System block diagram**

Each sample, including the GaAs module, is connected into a curve tracer that is composed of I-V measurement circuitry and a 4-bit resistor ladder curve tracer. Additionally, each sample, other than the GaAs module, is connected to a common-anode pixel multiplexer, allowing each of the six pixels fabricated onto the perovskite solar cell sample to be individually connected into the curve tracing circuitry or into a discharge circuit when not being actively

measured.

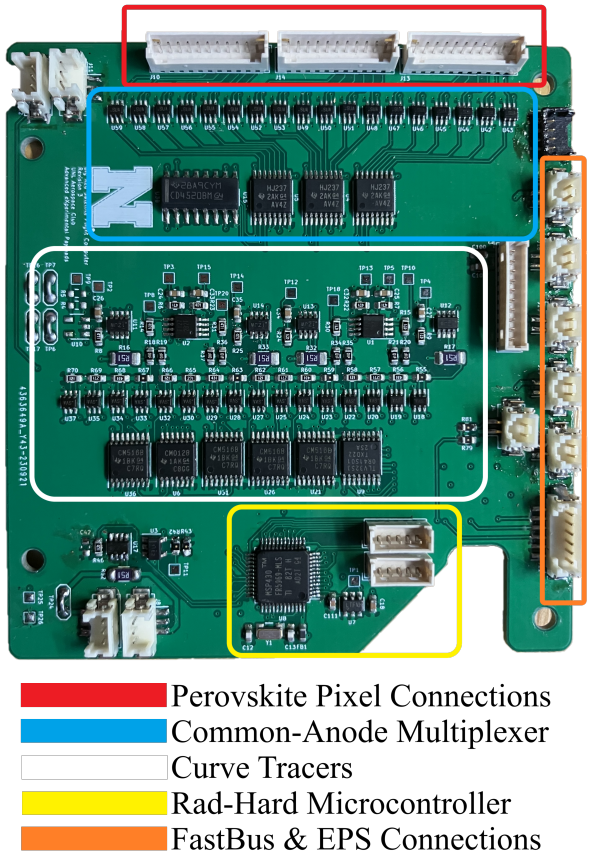


**Figure 3: Assembled instrumentation in 1U form factor**

As the chassis for the system, the NearSpace Launch 1U FastBus CubeSat Platform is used, along with its electrical power system (EPS) and EyeStar S4 satellite transmitter module, connected via the terminals labeled in orange in Figure 3. Integrated into the EPS is a central control system with eight semiconductor power switches for sequencing power to multiple connected devices. Through an integrated UART connection, the power switches can be controlled, and data can be sent to the radio for transmission. This platform also includes a set of batteries and GaAs solar panels on each face of the CubeSat connected into maximum power point trackers for charging.

In addition to these mentioned systems, a secondary set of sensors, dubbed the secondary payload, is integrated on a circuit board mounted above the flight computer. This circuit board contains a magnetometer, accelerometer, and gyroscope to monitor movement of the CubeSat while in orbit. Additionally, a terrestrial relay is mounted on this board that has a charging and discharging circuit connected to the normally open and normally closed terminals.

To operate this system, a radiation hardened microcontroller, the MSP430FR5969-SP, is connected to all mentioned subsystems with a simple firmware control loop for performing the mission, shown in Figure 3 labeled in yellow. Connected to this microcontroller is a LT6654AHS6-3.3 precision voltage reference that generates 3.299V with ±10ppm/°C temperature stability. These systems are visualized in the simplified block diagram shown in Figure 2. To allow programming and debugging of BRS-1 while assembled, a ten-pin Tag-Connect board was mounted on one face.

### *Perovskite Payload*

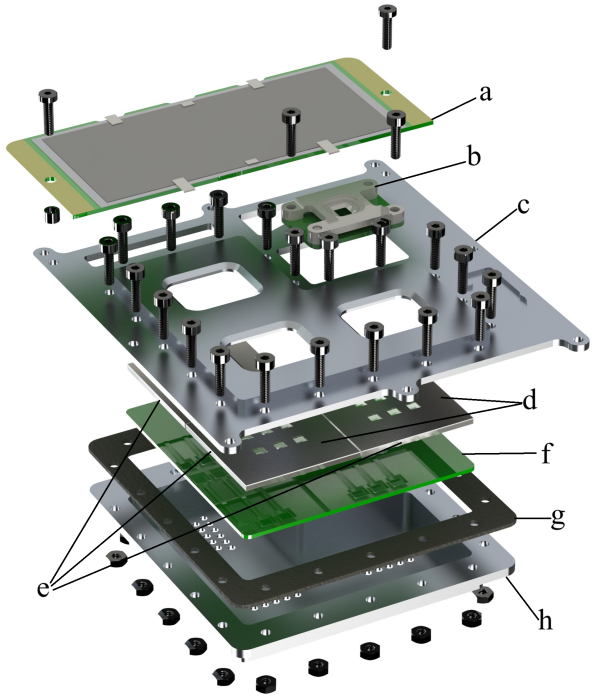


**Figure 4: Perovskite payload exploded view showing a) GaAs module, b) sun vector sensor, c) perovskite retention plate, d) perovskite light masks, e) perovskites, f) pogo pin contactor, g) gasket, h) bottom plate**

The machined aluminum payload, shown in Figure 4, consists of eight main components, in addition to the screws for assembly. Included on the outer face payload is the GaAs module, Figure 4a, and sun vector sensor, Figure 4b. The perovskite reten-

tion plate, Figure 4c, mounts the perovskite samples using MasterBond EP30-2 epoxy, a low outgassing, optically clear epoxy. Between the perovskites, Figure 4e, and the retention plate is a light mask, Figure 4d, which restricts the amount of light interacting with the perovskite active layer to a $0.058cm^2$ area.

Using EP30-2 epoxy, small circuit boards, Figure 5a, are mounted to the rear center of the perovskite samples. These circuit boards have an MCP9808 precision temperature sensor for monitoring the temperature of the sample glass. These sensors are configured and queried using an I2C connection. The perovskite ohmic contacts are electrically connected into the system using the contactor board, Figure 4f. Mounted to this contactor board is a set of pogo pins, Figure 5c, that are organized in the same layout as the ohmic contacts.

A pressurized seal is maintained using a thin, deformable gasket, Figure 4g. The entire payload is sealed using the bottom plate, Figure 4h, which has holes in it to allow a cable harness to escape from the payload, which is soldered into the contactor board. To monitor the pressurization while in orbit, Figure 5b, a small circuit board is included that has a BME280 humidity, pressure, and temperature sensor.

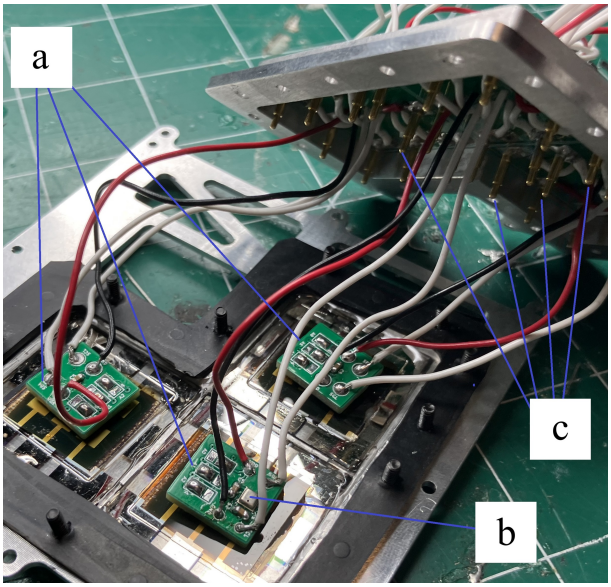


**Figure 5: Partial assembly of a test payload showing the a) MCP9808 sensing circuit boards, the b) BME280, and c) the pogo pins for electrically connecting the perovskite samples**

A separate cable harness is attached at the rear of each perovskite sample, which collects the ground signals for each pixel, the common anode, the I2C connections for the sensors, and power for the onboard sensors. These cable harnesses connect into the instrumentation using the connectors shown in red in Figure 3. Each conductor of the cable harness feeds through a hole in the bottom plate of the payload, which has a complimentary hole in the pogo pin contactor. The array of holes is inset to the outside face of the bottom plate, so that they can get potted using EP30-2 epoxy. By assembling the perovskite payload in a glovebox filled with an inert gas, the internal volume of the payload will be inert. This should encourage longevity of the samples after BRS-1 is integrated into NRCSD27 and waiting for launch in Florida.

### *Sun Vector Sensor*

One aspect of perovskite validation is ensuring the percent efficiency of the solar cells are maintained from manufacture to integration, to launch, and to deployment. The calculation of efficiency requires knowledge of the amount of light interacting with the active area of the solar cell, which can only be reliably accomplished using a sun vector sensor. Sun vector sensors perform high resolution measurements of the location of the sun in spherical coordinates, as defined by ISO 80000-2:20195, relative to the z-axis of the sensors' sensing face, shown in Figure 6.[18] By knowing the polar angle of the sun flux, $\theta$, and the approximate orbiting altitude of the CubeSat, the amount of light interacting with the perovskite solar cell can be calculated.

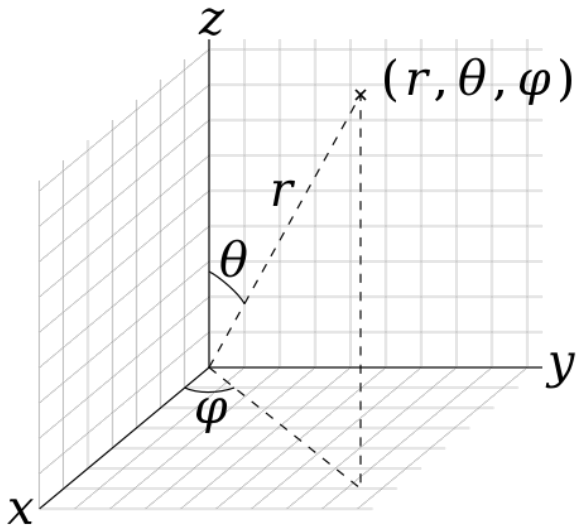


**Figure 6: Definition of spherical coordinates from ISO 80000-2:2019**

The selected sun vector sensor, the FSS100 Nano Fine Sun Sensor, is integrated to the system through

an I2C connection, allowing configuration and query of internal registers. This sensor is capable of 16 Hz measurements of the spherical coordinates representing the position of the brightest object on a calibrated four quadrant photodiode. Using the one-shot mode of the sensor, we can sample the sensor when we need the reading based on our GaAs trigger signal.

### *Curve Tracer*

Interfaced to each solar cell sample is a curve tracer that consists of an INA190-series current-shunt monitor measuring across a 510mΩ shunt resistor with a gain of 200. To measure the voltage developed by the sample, an OPA2387 operational amplifier was used as a unity gain buffer to prevent undue load on the sample. These were both connected upstream from a 4-bit resistor ladder, which was realized using a CD4516 up/down BCD counter, where the output bits control ADG841 CMOS single-pole, single-throw (SPST) switches, which either connected or bypassed a load resistor from the sample. Due to their very low on-resistance (0.28 mΩ typical) and the higher load resistance it was controlling relative to itself, by throwing the SPST switch the load resistance would be bypassed, minus a minimal offset current. By chaining these together in series using the BCD bits, a ladder of resistors can be used to create a configurable load resistance. This system is shown in Figure 3 labeled in white.

Utilizing the counter, the load resistance can be swept either forward or backward, allowing the hysteresis of the perovskite J-V curve to be observed. All four curve tracers are clocked synchronously, so all four samples can be traced together. To verify the curve tracer was operational, a 4012 NAND gate was connected to the LSB of the four counters, one for each sample including GaAs, and the output fed to a microcontroller pin. This circuitry, along with the MCP9808 and BME280 sensors, consumed 4mA at 3V3.

The short circuit condition is achieved by the activation of all SPST switches, where the sum of the on-resistance for four switches is 1.12Ω typical. The open circuit condition is achieved by placing a 1MΩ resistor on the MSB of the counter. While this reduces the curve resolution to $2^3 + 1$, it ensures that open circuit reliably generates $V_{OC}$.

When selecting resistors for the first three LSBs, it is important to consider how the ladder steps balance. For BRS-1 the resistor ladder consists of, from LSB to MSB, 120Ω, 270Ω, 430Ω, and 1MΩ. This results in a nearly linear increase in resistance for the first eight steps and then a large step to open circuit for the next eight steps. Each resistor was chosen to have automotive quality ratings, low temperature coefficients (±10ppm/°C), and low variability (±0.05%), ensuring that operation will be consistent when subject to temperature swings and different manufacturing batches. Each sample is connected to its own resistor ladder and the positive lead of the resistor ladder is connected to the common anode of the sample with the negative lead connected to system ground. Due to the limited number of ADC channels on the microcontroller, a 74CBTLV3253 analog multiplexer was used to 1-of-4 multiplex the voltage and current signals to two ADC channels. To control which sample is electrically visible to the measurement circuitry, a multiplexer was designed to control the ground leads of the pixels.

### *Common-Anode Pixel Multiplexer*

Each perovskite sample has its ground connections multiplexed to the microcontroller's system ground, providing the reference connection to acquire measurements. To accomplish this, each pixel ground is connected to the drain terminal of an ADG839 single-pole, double-throw (SPDT) semiconductor switch. The first throw is connected to the ground of the system and the second throw is connected to a discharge circuit. The ADG839 is designed with a low on-resistance, providing a 0.35Ω typical resistance and minimal distortion in the signal. Overall, including the resistance of the SPDT, SPST, and shunt resistor, the short circuit connection of a pixel has a 1.98Ω load, not accounting for the resistance of the copper traces. To operate these switches, a CD4518 4-bit BCD counter was connected to three CD74HC237 3:8 decoders, which were connected to the six switches for the pixel grounds. By clocking the counter, the pixel grounds could be cycled through synchronously for all three samples. To verify the multiplexer was operational, a 4012 NAND gate was connected to bit-6 of each decoder and the output fed to a microcontroller pin. This system is highlighted in Figure 3 in blue.

When the pixel ground connection is not connected to the system ground, the default state, it is connected into a "discharge" path, to prevent charge from accumulating in the substrate. Generally, this is accomplished by means of a discharge resistor, $R_{discharge}$ from Figure 2, which is ideally selected to place the pixel in its maximum power point.[19] Operating the unused pixel at this point on the curve has been shown to provide the highest longevity.[20]

During the development of this instrument, dif-

ficulties were encountered with disconnecting the pixel ground from system ground. Because the instrumentation is managing multiple connections, it would be expected for connections that are not selected by the multiplexer to hold no influence on the selected signal, within a given design margin. When testing the instrument with off-the-shelf, common-cathode, silicon solar cells, where the anodes are multiplexed on the positive terminal of the resistor ladder, this operation is demonstrated. When testing the instrument with common-anode, perovskite solar cells, the selected pixel would have an amplified J-V curve, much larger than the design margin of 1.7mV at open circuit and 2.1µA at short circuit per pixel. Commonly, the current density would rise above 70 milliamps per square millimeter, though this would depend on the state of the other pixels. This effect would disappear when the only physical connections were to the common-anode and a single pixel, as would be done when characterizing with a Keithley.

When $R_{discharge}$ was set to the maximum power point, the J-V curve would rise when the load resistance on the curve tracer was lower than $R_{discharge}$. Recalling 20, the second-best option for $R_{discharge}$ was short circuit. Replacing $R_{discharge}$ with a short provided no current density spikes and alleviated our issues and concerns. This heavily motivated the interest in using a mechanical relay for disconnection, which some automated solar cell characterization tools utilize. This circuitry, along with the microcontroller and various peripheral circuitry, consumed 3mA at 3V3.

### *Secondary Payload*

Many small sensors can be easily integrated into a 1U CubeSat form factor and, taking advantage of this fact, BRS-1 includes an accelerometer, gyroscope, and magnetometer. Monitoring the acceleration and rotation of the CubeSat provides a means to verify when it has detumbled. While not crucial, because the GaAs trigger and passive orientation due to the magnet, it can provide additional confidence in the design. Including a magnetometer provides additional confidence in the sun vector sensor, as the pointing direction of the CubeSat can be confirmed.

To provide this functionality, the ICM-20649 development board from Adafruit (product ID 4464) provided the accelerometer and gyroscope functions and the magnetometer function was provided by the MLX90393 development board from Adafruit (product ID 4022). Because these boards communicate over I2C, they can be easily integrated into the existing I2C bus used for the MCP9808 temperature sensors. These two development boards consumed 2.8mA at 3V3, with LEDs removed.

In addition to these included development boards, a terrestrial relay development board from Adafruit was incorporated (product ID 2923). Based on testing reported by NASA in Teverovsky 1999, relays used in spacecraft are more likely to fail due to the low-pressure conditions from an arc-at-break process.[21] But their testing was performed with a simulated 60V power bus, where the arcing condition is much more likely to happen. Considering the issues presented with the pixel multiplexer, we were interested in investigating the feasibility of replacing the semiconductor switches with physical contactors. Naturally, space-grade (hermetically sealed) relays are manufactured by various companies to prevent this issue, but they are bulky and expensive. For our system, the switching currents are very low, so it's likely that the arc-at-break process would be less likely to occur.

To test this idea, both the latching relay normally open (NO) and normally closed (NC) contacts were connected to an RC circuit with a $\tau_{charge}$ of 10 milliseconds and $\tau_{discharge}$ of 1 second. To energize these RC circuits, a 3V3 line was connected to the common terminal. The NO contact would be latched and sampled for 100 ADC samples. A five second delay would be completed to allow NC to discharge, after which the relay would be latched to NC and the same sampling process would be completed. The average voltage would be transmitted over the onboard radio and by tracking the voltage through the duration of the mission, failure mechanisms can be tracked and assessed. Contact damage would manifest as a reduced charge voltage and arcing would manifest as no voltage. In the case of the relay contact fusing to NO or NC, then the opposite contact would read close to the ground rail. This development board consumed 3µA at 3V3, with LEDs removed.

### *Passive Attitude Determination and Control*

After being deployed from the International Space Station, the CubeSat has an initial momentum imparted on it that can act upon any three of the axes randomly. This momentum needs to be removed from the system, which can be accomplished using magnetic torque.

Similar to the Quetzal-1 CubeSat as reported by Alvarez et al. 2023, BRS-1 incorporates an appropriately sized magnet to passively orient the antenna faces of the CubeSat with the Earth's magnetic field

line.[22] The magnet will exert a torque to align its poles with the Earth's poles that will transfer the deployment momentum to the primary axis of the magnet. This new rotational axis will cause the solar panels and sample face to be directed towards the sun. For BRS-1, the K&J Magnetics Catalog Number D84 was mounted to the inside of the antenna panel.

Using the GaAs trigger line, BRS-1 knows when it is aligned with the sun to trigger measurements. The combination of these two elements allows a passive attitude determination system to be achieved, which meets our mission needs.

### *Data Packet Format*

Using NearSpace Launch's EyeStar S4 radio modem allows only 17 bytes to be used for measurement data in a single packet. Given that the S4 radio modem uses the Iridium constellation for data transmission, along with our passive attitude determination system, it is likely that we will drop packets. For this reason, we designed the data from each mission component to fit into a single packet. The J-V curve data would fit into 16 bytes, with 8-bit ADC readings for the voltage and current at the first eight points. The sun vector sensor data and temperature data would fit into 16 bytes. The gyroscope, magnetometer, and relay data would fit into 16 bytes and the accelerometer and BME280 data would fit into 16 bytes. Each of these packets would be appended with a status byte that indicates which packet type it is (2 bits), which sample is selected (2 bits), which pixel is selected (3 bits), and which direction the J-V sweep was performed (1 bit). To improve the likelihood that we will receive any given packet of data, each packet is transmitted twice.

### *Firmware Control Loop*

The firmware was prepared using the Energia integrated development environment (IDE), adapted by Texas Instruments from the Arduino IDE. At startup, the processor will reset the curve tracers by clocking them until the NAND gate indicates they are all set to 0x1. The multiplexer reset line is toggled at startup, so the same pixel is characterized for each sample. The trace direction is also set to reverse, which is from open circuit to short circuit. The ADC is configured to read at 8-bit resolution and use the external voltage reference. Then the processor configures the UART interface to the FastBus EPS and waits until the BUSY line is no longer asserted. Then, a packet is sent to turn on the auxiliary power lines connected to the instrumentation. Finally, the instrumentation is configured over the I2C channel.

The processor then enters the main loop, where the curve tracers are reset again and set to forward tracing, and the system starts waiting for the GaAs trigger line to be asserted. By placing the curve tracers in forward mode and resetting them, the GaAs would be in open circuit, providing the conditions necessary for the comparator trigger.

During this waiting period, the processor will send a packet to the FastBus EPS to keep all power switches engaged. The FastBus EPS will shut down the connected power lines if it does not receive a packet in a five-minute window, which ensures that any hangups in the instrumentation will not end the mission. Once the trigger line is asserted, the curve tracing direction is set to reverse and reset again. The sun vector sensor is configured for one-shot mode and a sample is collected. Then, the curve tracer is clocked, and on each clock the voltage and current from each sample is collected by cycling through the analog multiplexer on the curve tracer output lines. Once all sixteen steps have been completed, the trace direction is inverted and if the trace direction is back to reverse, the pixel multiplexer is clocked, moving onto the next pixel. If the pixel multiplexer NAND gate is asserted, indicating all pixels have been sampled, then the multiplexer is reset. The ladder is reset again. Then the temperatures on the samples are acquired, the BME280 readings are collected, the accelerometer, gyroscope, and magnetometer readings are collected, and the relay test cycle is completed.

After this sampling period is complete, the data is packaged into their packets, and they are transmitted twice through the connected EyeStar S4 radio modem. The process loops from here, continually incrementing through pixels, sampling, transmitting, and then waiting to see the sun again.

For all mentioned operations, especially the I2C operations, it is ensured that none are blocking functions. If they were blocking, then any hangup in an I2C transaction could halt our operations, which was a situation reported by Aguilar-Nadalini et al. 2023[23] and Zea et al. 2023.[24] In their satellite, the connected heaters stopped communicating and the system eventually ran out of power and could not reboot. While the FastBus EPS should power cycle our instrumentation, we wanted to ensure that any permanent hangup, such as an issue from launch, would not stop our mission from operating.

## PRE-LAUNCH PERFORMANCE

Prior to the Sine Sweep and Random Vibration test, BRS-1 was permanently assembled. EP30-2 epoxy was applied to all moving joints, such as cable connectors and screws. This ensured that nothing would come lose and cause a failure condition for the test, causing the mission to slip. This test performs a sine sweep from 5 – 2000 Hz with a 0.5g peak and two octaves per minute on each axis. Then, a random vibration test consisting of 20 – 2000Hz with 5.757g peak forces for 1 minute in each axis is performed. After this, another sine sweep is performed. The data from these tests can be analyzed to show any spikes in the spectral density of the acceleration, indicating loose or separated components. This provides a strong indication of success during launch.

After performing the vibration test, the BRS-1 perovskite solar cells were performance tested to assess if any damage had occurred. Using the onboard instrumentation, J-V curves were extracted through the debugging connector. With a custom bracket mounted to an Ossila Solar Simulator (Ossila product code G2009B1), an AM1.5 spectrum is generated and directed onto the perovskite sample face with a $100mW/cm^2$ illumination.

### *Assembly Results*

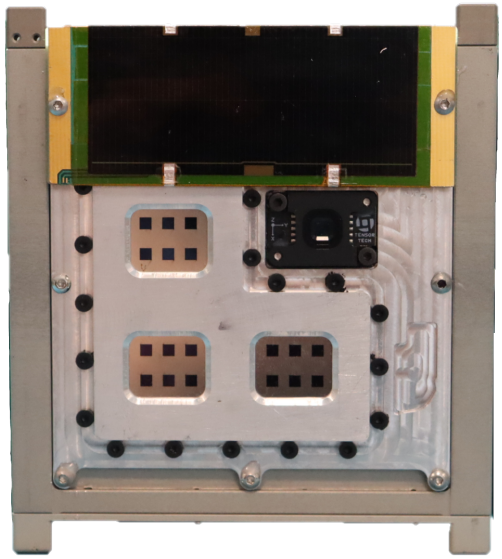

**Figure 7: Head-on picture of BRS-1 solar cell face**

After assembling BRS-1 and epoxying the joints, the subsystems were tested for nominal operation. The only failure that was observed was on the sun vector sensor. During epoxying, the slim connector for this sensor had epoxy seep into its socket and surround the contact, rendering the sensor unusable. Due to time restrictions, we were not able to rectify the problem. Because of this, it is not expected that the sun vector sensor will operate in-orbit, limiting the ability to estimate irradiance.

Additionally, the perovskite payload prepared for flight was tested in a vacuum chamber to assess its ability to maintain its internal pressurized volume. This test indicated that it could not hold pressure and quickly evacuated its internal volume. Due to the addition of encapsulation to the perovskite solar cells, it was determined that the pressurized volume was a redundancy and moved forward without it. The final satellite that was prepared for launch is shown in Figure 7.

### *Final Perovskite Performance*

Each perovskite pixel was characterized while illuminated by an AM1.5 $100mW/cm^2$ light source at fabrication, after shipment, and before launch. These results are tabulated in Table 1, Table 2, and Table 3. While working with the assembled BRS-1, a strong hysteresis was noticed on the samples, where the performance when swept forward ($V_{oc}$ to $J_{sc}$) versus reverse ($J_{sc}$ to $V_{oc}$) strongly varied. Due to this, both directions are reported for the Post Vibe Test performance. Additionally, there are multiple pixels that were reported to be dead at fabrication that were alive after shipping or alive after integration into BRS-1. This is due to the coverslip epoxy, which would cover some contacts and require careful placement of electrodes to characterize. Two of the samples, X018 and X016, were manufactured by the National Renewable Energy Laboratory with a $Cs_{0.05}(FA_{0.95}MA_{0.05})_{0.95}Pb(I_{0.95}Br_{0.05})_3$ composition and $(FAPbI_3)_{0.95}(MAPbBr_3)_{0.05}$ composition, respectively. The third sample, X002, was manufactured by Swift Solar with a proprietary composition.

## FUTURE OPPORTUNITIES

While the developments of BRS-1 provide a great baseline for future missions, there are many opportunities to improve on it. By adding an active curve tracer, the perovskite solar cells would be able to have their dark current properties investigated, including the calculation of series resistance can be performed.[12] Additionally, if a magnetorquer is included, the samples can be actively oriented towards the sun, providing measurements at elevated temperatures. Considering the limitations of using the Iridium constellation, it may be beneficial to use

**Table 1: Tabulated performance characteristics for the X018 perovskite solar cell sample, manufactured by NREL, showing changes in performance from fabrication, to shipment, to integration for launch**

| X018 Performance | | | | | |
|---|---|---|---|---|---|
| | | | | Post Vibe Test | |
| Pixel | Metric | Fabrication | Shipment | Forward | Reverse |
| 0 | $FF$ | 67.5 | 62.9 | 65.8 | 81.9 |
| | $V_{oc}$ | 1089.0 | 994.0 | 980.5 | 851.5 |
| | $J_{sc}$ | 22.2 | 28.1 | 26.2 | 26.2 |
| | $PCE$ | 16.3 | 17.6 | 16.9 | 18.3 |
| 1 | $FF$ | 0.0 | 64.9 | 72.1 | 79.9 |
| | $V_{oc}$ | 0.0 | 980.1 | 954.7 | 851.5 |
| | $J_{sc}$ | 0.0 | 28.0 | 26.2 | 24.0 |
| | $PCE$ | 0.0 | 17.8 | 18.0 | 16.3 |
| 2 | $FF$ | 74.4 | 65.0 | 68.2 | 79.9 |
| | $V_{oc}$ | 1096.0 | 973.7 | 980.5 | 851.5 |
| | $J_{sc}$ | 22.5 | 27.6 | 24.0 | 24.0 |
| | $PCE$ | 18.5 | 17.4 | 16.0 | 16.3 |
| 3 | $FF$ | 74.3 | 64.9 | 65.4 | 83.2 |
| | $V_{oc}$ | 1095.0 | 978.5 | 967.6 | 838.6 |
| | $J_{sc}$ | 22.5 | 27.4 | 28.4 | 26.2 |
| | $PCE$ | 18.4 | 17.4 | 18.0 | 18.3 |
| 4 | $FF$ | 68.4 | 63.3 | 71.8 | 74.5 |
| | $V_{oc}$ | 1085.0 | 974.6 | 954.7 | 851.5 |
| | $J_{sc}$ | 22.5 | 27.3 | 26.2 | 26.2 |
| | $PCE$ | 16.7 | 16.8 | 18.0 | 16.6 |
| 5 | $FF$ | 73.3 | 53.7 | 59.2 | 73.9 |
| | $V_{oc}$ | 1089.0 | 991.4 | 980.5 | 799.9 |
| | $J_{sc}$ | 22.2 | 27.7 | 26.2 | 26.2 |
| | $PCE$ | 16.3 | 14.8 | 15.2 | 15.5 |

**Table 2: Tabulated performance characteristics for the X016 perovskite solar cell sample, manufactured by NREL, showing changes in performance from fabrication, to shipment, to integration for launch**

| X016 Performance | | | | | |
|---|---|---|---|---|---|
| | | | | Post Vibe Test | |
| Pixel | Metric | Fabrication | Shipment | Forward | Reverse |
| 0 | $FF$ | 69.4 | 74.6 | 76.7 | 83.8 |
| | $V_{oc}$ | 863.0 | 1020.0 | 993.5 | 903.1 |
| | $J_{sc}$ | 24.3 | 29.2 | 28.4 | 26.2 |
| | $PCE$ | 14.6 | 22.2 | 21.6 | 19.8 |
| 1 | $FF$ | 68.5 | 74.8 | 0.0 | 0.0 |
| | $V_{oc}$ | 785.0 | 1025.0 | 129.0 | 0.0 |
| | $J_{sc}$ | 24.6 | 28.8 | 0.0 | 0.0 |
| | $PCE$ | 13.2 | 22.1 | 0.0 | 0.0 |
| 2 | $FF$ | 78.1 | 33.3 | 77.9 | 80.4 |
| | $V_{oc}$ | 1022.0 | 14.4 | 877.3 | 799.9 |
| | $J_{sc}$ | 24.5 | 5.4 | 28.4 | 28.4 |
| | $PCE$ | 19.6 | 0.0 | 19.4 | 18.2 |
| 3 | $FF$ | 79.5 | 0.0 | 0.0 | 0.0 |
| | $V_{oc}$ | 1031.0 | 0.0 | 245.1 | 0.0 |
| | $J_{sc}$ | 24.4 | 0.0 | 0.0 | 0.0 |
| | $PCE$ | 20.0 | 0.0 | 0.0 | 0.0 |
| 4 | $FF$ | 0.0 | 75.2 | 66.8 | 87.2 |
| | $V_{oc}$ | 0.0 | 1005.9 | 864.4 | 787.0 |
| | $J_{sc}$ | 0.0 | 24.2 | 30.5 | 26.2 |
| | $PCE$ | 0.0 | 21.8 | 17.6 | 18.0 |
| 5 | $FF$ | 77.2 | 74.0 | 71.6 | 87.3 |
| | $V_{oc}$ | 1002.0 | 1021.0 | 903.1 | 812.8 |
| | $J_{sc}$ | 24.5 | 29.2 | 30.5 | 28.4 |
| | $PCE$ | 19.0 | 22.1 | 19.8 | 20.1 |

**Table 3: Tabulated performance characteristics for the X002 perovskite solar cell sample, manufactured by Swift Solar, showing changes in performance from fabrication, to shipment, to integration for launch**

| X002 Performance | | | | | |
|---|---|---|---|---|---|
| | | | | Post Vibe Test | |
| Pixel | Metric | Fabrication | Shipment | Forward | Reverse |
| 0 | $FF$ | 0.0 | 0.0 | 63.5 | 76.5 |
| | $V_{oc}$ | 0.0 | 0.0 | 916.0 | 799.9 |
| | $J_{sc}$ | 0.0 | 0.0 | 24.0 | 24.0 |
| | $PCE$ | 0.0 | 0.0 | 14.0 | 14.7 |
| 1 | $FF$ | 0.0 | 37.2 | 68.6 | 69.6 |
| | $V_{oc}$ | 0.0 | 991.4 | 799.9 | 722.5 |
| | $J_{sc}$ | 0.0 | 21.0 | 24.0 | 26.2 |
| | $PCE$ | 0.0 | 9.2 | 13.2 | 13.2 |
| 2 | $FF$ | 79.6 | 70.6 | 0.0 | 0.0 |
| | $V_{oc}$ | 1119.0 | 1074.9 | 0.0 | 0.0 |
| | $J_{sc}$ | 21.1 | 25.9 | 0.0 | 0.0 |
| | $PCE$ | 18.8 | 19.7 | 0.0 | 0.0 |
| 3 | $FF$ | 0.0 | 54.8 | 64.9 | 76.0 |
| | $V_{oc}$ | 0.0 | 1047.0 | 812.8 | 722.5 |
| | $J_{sc}$ | 0.0 | 25.9 | 24.0 | 24.0 |
| | $PCE$ | 0.0 | 15.0 | 12.7 | 13.2 |
| 4 | $FF$ | 73.2 | 100.0 | 0.0 | 0.0 |
| | $V_{oc}$ | 1105.0 | 0.0 | 0.0 | 0.0 |
| | $J_{sc}$ | 21.2 | 4.5 | 0.0 | 0.0 |
| | $PCE$ | 17.1 | 0.0 | 0.0 | 0.0 |
| 5 | $FF$ | 0.0 | 73.9 | 78.1 | 87.9 |
| | $V_{oc}$ | 0.0 | 1086.0 | 825.7 | 748.3 |
| | $J_{sc}$ | 0.0 | 21.9 | 26.2 | 26.2 |
| | $PCE$ | 0.0 | 20.8 | 16.9 | 17.2 |

VHF HAM radio bands for improved data resolution and increased reliability. There are limitations to what can be extracted from J-V measurements and other sensors may be useful to further characterize performance of perovskite solar cells.

Radiation dosimeters can track the cumulative exposure to various types of space radiation (e.g., gamma rays, protons), which can give direct insight into failure mechanisms in space. A system to measure the external quantum efficiency (EQE) or spectral response of the solar cells helps in understanding their wavelength-dependent efficiency. This setup includes: a broad spectrum light source, monochromator to provide light of specific wavelengths, and a lock-in amplifier to enhance the signal-to-noise ratio for accurate measurements. Additionally, sensors to monitor environmental conditions such as temperature, pressure, and humidity (though low in space) are important for correlating the solar cell performance with ambient conditions. Finally, measurements including the photoluminescence, electroluminescence, reflectance and transmittance of the solar cells, which provides insight into the optical properties and any changes in such properties induced due to the environmental effects in space. New generated defect states in the absorber material and any change in the band gap can be monitored using these techniques.

Given the low sun exposure area of a 1U CubeSat, it may be beneficial to scale up. Using a 2U or 3U CubeSat would provide a greater surface area to include more and varied perovskite solar cells. There are other potential satellite platforms as well, such as DiskSats, that provide a large, flat surface that can be outfitted with perovskites. Considering a DiskSat provides this flat surface, this would be beneficial for the current generation of perovskite solar cells, which are made on a quartz substrate.

There are numerous other approaches that have been considered for perovskite solar cells. Some researchers are developing flexible perovskite solar cells that are printed on large sheets. Other are developing tandem cells where the perovskite solar cell is one layer of a stack that incorporates other solar cells, such as GaAs, which allows multiple portions of the light spectrum to be simultaneously captured.

## SUMMARY

Big Red Sat-1, shown in Figure 7, is a 1U CubeSat that determines the performance of perovskite solar cells while in low earth orbit, for the purpose of assessing their technology readiness level. Using custom instrumentation, the perovskite solar cell pixels can be characterized through their J-V curve and analyzed on the ground, demonstrating their ability to operate in space. With a physical twin of the payload, the performance will be validated and failure mechanisms able to be examined. Based on these results, which will be fully collected by 17 July 2024, we will set a guidepost for future satellites designed to examine perovskite solar cells.

All custom designs for BRS-1 have been made open-source and publicly available on GitHub, with appropriate licensing. The licenses are CERN-OHL-S-2.0 for hardware, MIT for software, and CC BY-SA 4.0 for documentation. This will allow future teams to examine and improve our designs and speed up development. This also provides these teams an opportunity to expand the included instrumentation to cover areas that we have not covered. Moving forward, it would be useful to add active curve tracing into the system, allowing characterization without active sun exposure. Active attitude determination and control systems would be useful for testing how the samples perform when their temperature is increased by pointing them directly at the sun for an extended period. Additionally, new architecture of perovskite solar cells can be explored, including tandem cells where they combine GaAs and perovskite layers to increase their efficiency. This could also include flexible perovskite solar cells, which may provide more convenient methods of affixing them to a monitoring circuit. Because BRS-1 is such a low-power satellite, many different systems could be incorporated without ruining the power budget.

Getting to this point in development, where it has been launched and deployed, took over three years of consistent work. Our project was created as a collaboration between middle school, high school, and UNL students, where the primary goal was to get the middle and high school students involved in aerospace related projects within their own state. Many of these students have graduated and moved onto high school or undergraduate degrees. Some of the undergraduate students at UNL have gone on to graduate degrees and into industry. If they stay in the aerospace industry, then they may be back to report their work on next-generation perovskite solar cell satellites.

## ACKNOWLEDGMENTS

In addition to individual donors, major support was provided by NASA, the University of Nebraska College of Engineering, the Rogers Foundation, the Cooper Foundation, the Millard Public Schools Foundation, Monolith, the Ethel S. Ab-

bott Foundation, the Acklie Charitable Foundation, NASA Nebraska Space Grant, the University of Oklahoma, the National Renewable Energy Laboratory, Ameritas, and Shirts 101.

The Big Red Sat Team included University of Nebraska-Lincoln (UNL) graduate and undergraduate students and middle and high school members. Key and core members not previously recognized include UNL undergraduates participants: John Helzer, MJ Schuster, Michael Hackett, Hailey Anderson, Samuel Atkins, Andrew Duweling, Benjamin Finnegan, Alyssa Simpson; students starting in high or middle school (progression as noted): Emma Walter (Bellevue East HS/UNL), Brett Bailey (Bellevue West HS), Victoria Bardon Soto (Burke HS/University of Chicago), Gavin Luthi and Dylan Smith (Greta HS), Nikhil Woods (Lewis & Clark MS/Brownell Talbot),Elsa Meyer (Lincoln East HS/University of Iowa), Tiegan Gunning (Lincoln HS/UNL), Caleb Meyer, Kaycee Meyer, and Andrew Wing (Lincoln Lutheran HS), Evan Tyler (Lincoln North Star HS), Andrew Flaugh (Millard North HS), Lydia Dominy (Norris MS), Brooks Bossard (Norris MS/HS).

## References

[1] NASA Jet Propulsion Laboratory. Chapter 11. typical onboard systems, electrical power supply and distribution subsystems, 2008.

[2] Akihiro Kojima, Kenjiro Teshima, Yasuo Shirai, and Tsutomu Miyasaka. Organometal halide perovskites as visible-light sensitizers for photovoltaic cells. *Journal of the american chemical society*, 131(17):6050–6051, 2009.

[3] National Renewable Energy Laboratory. Best research-cell efficiency chart, 2024.

[4] Lyndsey McMillon-Brown, Joseph M Luther, and Timothy J Peshek. What would it take to manufacture perovskite solar cells in space?, 2022.

[5] Sidra Khatoon, Satish Kumar Yadav, Vishwadeep Chakravorty, Jyotsna Singh, Rajendra Bahadur Singh, Md Saquib Hasnain, and SM Mozammil Hasnain. Perovskite solar cell's efficiency, stability and scalability: A review. *Materials Science for Energy Technologies*, 2023.

[6] Rabia Sharif, Arshi Khalid, Syed Waqas Ahmad, Abdul Rehman, Haji GHualm Qutab, Hafiz Husnain Akhtar, Khalid Mahmood, Shabana Afzal, and Faisal Saleem. A comprehensive review on the current progress and material advances in perovskite solar cells. *Nanoscale Advances*, 2023.

[7] Nam Joong Jeon, Jun Hong Noh, Woon Seok Yang, Young Chan Kim, Seungchan Ryu, Jangwon Seo, and Sang Il Seok. Compositional engineering of perovskite materials for high-performance solar cells. *Nature*, 517(7535):476–480, 2015.

[8] Yu Miyazawa, Masashi Ikegami, Hsin-Wei Chen, Takeshi Ohshima, Mitsuru Imaizumi, Kazuyuki Hirose, and Tsutomu Miyasaka. Tolerance of perovskite solar cell to high-energy particle irradiations in space environment. *IScience*, 2:148–155, 2018.

[9] Min Chen, Yifan Dong, Yi Zhang, Xiaopeng Zheng, Gabriel R McAndrews, Zhenghong Dai, Qi Jiang, Shuai You, Tuo Liu, Steven P Harvey, et al. Stress engineering for mitigating thermal cycling fatigue in perovskite photovoltaics. *ACS Energy Letters*, 9:2582–2589, 2024.

[10] Biruk Alebachew Seid, Sema Sarisozen, Francisco Peña-Camargo, Sercan Ozen, Emilio Gutierrez-Partida, Eduardo Solano, Julian A Steele, Martin Stolterfoht, Dieter Neher, and Felix Lang. Understanding and mitigating atomic oxygen-induced degradation of perovskite solar cells for near-earth space applications. *Small*, page 2311097, 2024.

[11] Ahmad R Kirmani, David P Ostrowski, Kaitlyn T VanSant, Todd A Byers, Rosemary C Bramante, Karen N Heinselman, Jinhui Tong, Bart Stevens, William Nemeth, Kai Zhu, et al. Metal oxide barrier layers for terrestrial and space perovskite photovoltaics. *Nature Energy*, 8(2):191–202, 2023.

[12] Daniel Abou-Ras, Thomas Kirchartz, and Uwe Rau. *Advanced characterization techniques for thin film solar cells*, volume 2. Wiley Online Library, 2011.

[13] Ilaria Cardinaletti, Tim Vangerven, Steven Nagels, Rob Cornelissen, Dieter Schreurs, Jaroslav Hruby, Jelle Vodnik, Dries Devisscher, Jurgen Kesters, Jan D'Haen, et al. Organic and perovskite solar cells for space applications. *Solar Energy Materials and Solar Cells*, 182:121–127, 2018.

[14] YongGuang Tu, GuoNing Xu, XiaoYu Yang, YiFei Zhang, ZhaoJie Li, Rui Su, DeYing Luo, WenQiang Yang, Ying Miao, Rong Cai, et al. Mixed-cation perovskite solar cells in space. *Science China. Physics, Mechanics & Astronomy*, 62(7):974221, 2019.

[15] William Delmas, Samuel Erickson, Jorge Arteaga, Mark Woodall, Michael Scheibner, Timothy S Krause, Kyle Crowley, Kaitlyn T VanSant, Joseph M Luther, Jennifer N Williams, et al. Evaluation of hybrid perovskite prototypes after 10-month space flight on the international space station. *Advanced Energy Materials*, 13(19):2203920, 2023.

[16] Luca Prudenzia, Alessio Prosperia, Fernando Aranda Romeroa, Etienne Beierb, Chiara Pasquarielloa, Marco Giugliarellia, Kotish Grovera, and Felix Langc. Long-term in-orbit testing of perovskite solar cells on a 1u cubesat: an open-source design approach. 2023.

[17] Izrael Zenar C Bautista, Shuzhang Yang, Aekjira Kuyyakanont, Minoru Iwata, Tingli Ma, and Mengu Cho. Perovskite solar cells in space: Evaluation of perovskite solar cell hole transport material in space environment. *Transactions of the Japan Society for Aeronautical and Space Sciences*, 65(2):95–107, 2022.

[18] International Organization for Standardization. Iso 80000-2:20195, 2021.

[19] Tae-Youl Yang, Nam Joong Jeon, Hee-Won Shin, Seong Sik Shin, Young Yun Kim, and Jangwon Seo. Achieving long-term operational stability of perovskite solar cells with a stabilized efficiency exceeding 20% after 1000 h. *Advanced Science*, 6(14):1900528, 2019.

[20] Konrad Domanski, Essa A Alharbi, Anders Hagfeldt, Michael Grätzel, and Wolfgang Tress. Systematic investigation of the impact of operation conditions on the degradation behaviour of perovskite solar cells. *Nature Energy*, 3(1):61–67, 2018.

[21] Alexander Teverovsky. Relay failures specific to space applications. In *ISTFA 1999*, pages 285–292. ASM International, 1999.

[22] Dan Alvarez, Aldo Aguilar-Nadalini, José Bagur, Víctor Ayerdi, and Luis Zea. Design and on-orbit performance of the attitude determination and passive control system for the quetzal-1 cubesat. *J. Small Satell*, 12(2):1231–1247, 2023.

[23] Aldo Aguilar-Nadalini, Kuk H Chung, Cecilia Marsicovetere, José A Bagur, Juan F Medrano, Emilio Miranda, Víctor Ayerdi, and Luis Zea. Design and on-orbit performance of the electrical power system for the quetzal-1 cubesat. *J. Small Satell*, 12(2):1201–1229, 2023.

[24] Luis Zea, Aldo Aguilar-Nadalini, Marvin Martínez, Johan Birnie, Emilio Miranda, Fredy España, Kuk Chung, Dan Álvarez, José Antonio Bagur, Carlo Estrada, et al. Academic development and space operations of a multispectral imaging payload for 1u cubesats. *Journal of Applied Remote Sensing*, 17(4):047501–047501, 2023.